STRUCTURE AND FRACTURE VISUALIZATION OF TILTED ABS SPECIMENS PROCESSED VIA FUSED FILAMENT FABRICATION ADDITIVE MANUFACTURING

D. Richkov[1], Y. Rosenthal[1], D. Ashkenazi[2*], A. Stern[1,3]

[1]School of Mechanical Engineering, Afeka Academic College of Engineering, Tel Aviv, 69107, Israel
[2]School of Mechanical Engineering, Tel Aviv University, Ramat Aviv 6997801, Israel
[3]Department of Materials Engineering, Ben-Gurion University of the Negev, Beer Sheva 8410501, Israel
*Corresponding author's e-mail address: dana@eng.tau.ac.il

ABSTRACT

Fused filament fabrication (FFF) technique is one of the most frequently used additive manufacturing (AM) technologies for printing ABS and many other thermoplastic materials. The anisotropy of the mechanical properties of 3D-printed parts manufactured by FFF technology is still of major concern when using this technique. Thus, the component's orientation, build strategy and printing parameters affect the mechanical properties, and failure mechanisms are of crucial importance. This research aims to partly fill this gap by studying the structure and mechanical behavior of FFF-ABS specimens, and by performing fracture surface analysis by the three-point bend flexural test. A series of tests were conducted to determine the flexural properties of tilted specimens at 0°, 15°, 30°, 45°, 60° and 75° inclination angles relative to the machine platform. The work describes manufacture method of the specimens, experimental procedures, and outcomes from the mechanical and structural characterizations of the FFF-ABS specimens. Overall, two main failure modes were observed for the tested specimens: (1) inter-layer/ inter-raster bond failure (typical for upright specimens) and (2) intra-layer/trans-raster failure (typical for on-edge specimens). A mixed inter-layer/ intra-layer mode was found for the specimens tilted in-between the 15° and 60° range.

KEYWORDS: ABS polymer, additive manufacturing (AM), fused filament fabrication (FFF), mechanical properties, three-point bend test, fractography, fracture visualization.

1. INTRODUCTION

Fused filament fabrication (FFF) is one of the most broadly accessible additive manufacturing (AM) technologies, due to its low cost, wide range of available materials and the ability to produce complex geometries inexpensively [1]-[9]. The FFF technique is now used for fabricating low volume as load-carrying functional parts for many applications in robotics, medical, aeronautical, electronics, and automotive sectors. Despite the many benefits of AM technologies, building parts employing the FFF technique is quite challenging because it has various processing parameters that affect the mechanical properties, printed part quality, dimensional accuracy, and build time. These FFF processing parameters include build orientation, infill percentage, layer thickness, air gap and raster angle [10]. The relatively low mechanical properties of the FFF printed components are still a major limitation of the technique [1]-[9]. Out of many thermoplastic materials suited for FFF technology, the most broadly used and frequently researched polymer is the tough and strong amorphous acrylonitrile butadiene styrene (ABS). ABS is essentially a styrene-acrylonitrile copolymer modified by butadiene rubber. ABS combines the resilience of polybutadiene with the hardness and rigidity of polyacrylonitrile and polystyrene. ABS filaments are relatively inexpensive to produce and can be processed at relatively low temperatures (about 170 to 270 °C). The FFF printing process starts by extruding liquefied ABS filament in a prescribed manner on top of an existing layer with a preset specific build strategy, creating a two-dimensional layer (Fig. 1). The layer's deposited contour beads form the outermost and innermost edges of the part. The beads which are extruded inside the contour beads generate the cross-sectional layer of the part and are known as rasters [1]-[6]. Upon deposition, the raster rapidly heats the initial

Date of submission/acceptance: 08.11.2021/15.12.2021 https://doi.org/10.35219/awet.2021.01

build-up rasters and simultaneously cools, forming local bonds (inter-layers and intra-layers) by molecular diffusion (Fig.1) [11]. The inter-layers and intra-layers bond strength depends on the local temperature between adjacent rasters as determined by the dynamics of the molten polymer that governs the diffusion rate [12]-[15].

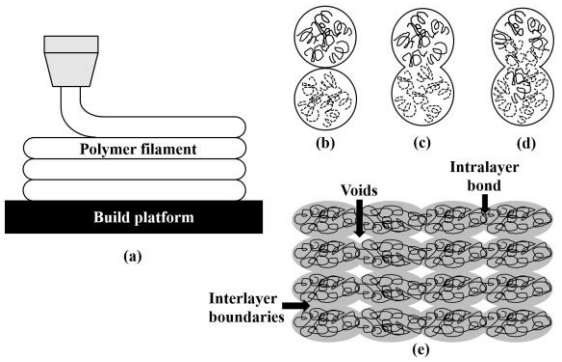

Fig. 1. Bond formation process for the AM-FFF technology: (a) the polymer filament layers; (b) surface contacting between two filament layers; (c) necking growth; (d) diffusion at the interface between two layers; and (e) the inter-layer and intra-layer bonding

The mechanical properties of FFF parts depend on the thermoplastic polymer properties, the product's geometric details, the FFF process parameters and they are expected to be anisotropic because of the inherent layered structure. The bonds between rasters and between layers result in the anisotropic properties of the printed part, with the highest strength in the longitudinal direction (parallel to the direction of printing), and the weakest strength in the z-axis direction between layers. So far, no material model has been capable of considering the dissimilar material behavior of ABS between tension and compression and an advanced and complex constitutive material model is highly required [1]-[9], [12]-[16]. It has been widely publicized that the typical defects found in the printed parts are poor bonding between rasters inside and in between the layers, porosity located between the rasters and porosity between the contour beads and rasters [1]-[9], [12], [16], [17]. Contact pressure is a critical determinant of the bond strength; higher contact pressures leading to larger contact surface area, provide improved mechanical properties. This study is part of on-going research [3], [16]-[17], seeking to advance knowledge about the mechanical properties, structure, and fracture behavior of FFF-ABS parts by using a three-point flexural test method. The main reason for choosing the three-point flexural bend method over a four-point test method is that the maximum flexural stress appears under the loading nose in this method, while the maximum bend stress is spread over the section of the specimen between the loading points in the four-point bend tests.

Printing parameters, such as extrusion temperature, layer height and interlayer structures have a noteworthy effect on fracture resistance and fracture behavior of AM FFF-ABS specimens. According to the literature, the essential energy for crack propagation across lamina is nearly an order of magnitude greater than the essential energy for crack propagation along lamina [18].

This study aims to examine the structure and mechanical behavior of FFF-ABS three-point flexural test specimens by performing fracture surface analysis. To that end, a series of tests were conducted to determine the flexural properties of tilted specimens at 0°, 15°, 30°, 45°, 60° and 75° inclination angles relative to the machine platform. This work describes the manufacture method of the specimens, experimental procedures, and outcomes from the structural and mechanical characterization of the FFF-ABS specimens, including the typical failure modes.

2. EXPERIMENTAL PART

2.1. Specimens

The ABS bend test specimens (127 mm × 12.7 mm × 3.2 mm) (Fig. 2) were printed on a STRATASYS© Dimension Elite© FFF machine on two separate trays at the following inclination angles: 0°, 15°, 30°, 45°, 60° and 75°, three specimens for each orientation (Fig. 3). For that purpose, an ABSplus filament (1.75 mm diameter) produced by Stratasys was used in the current work. The print parameters are based on the filament producer's (Stratasys) recommendations. The chosen 3D-printed specimen is a simple rectangular beam with specified geometry and dimensions according to ASTM D790 and ISO 178.

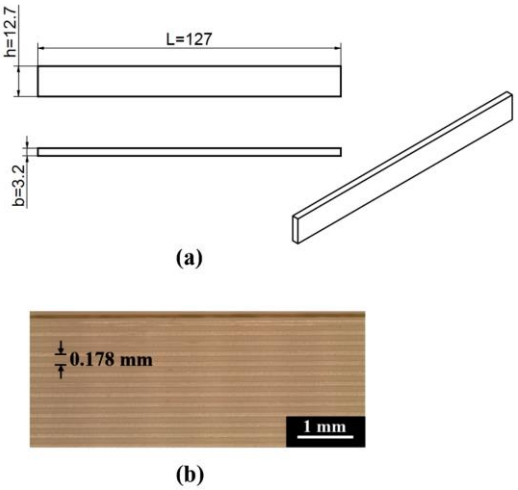

Fig. 2. ABS bend test specimen printed on the STRATASYS© Dimension Elite© FFF machine; (a) the dimensions of the specimen (127 mm × 12.7 mm × 3.2 mm); and (b) layer thickness of 0.178 mm

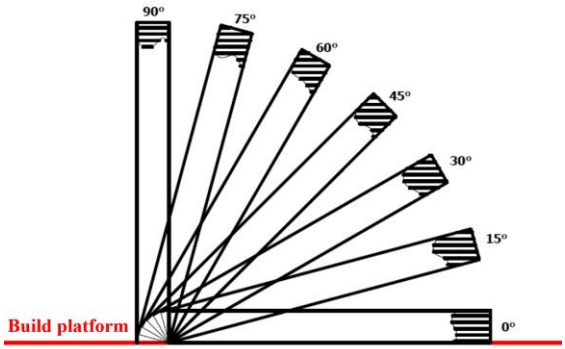

Fig. 3. The AM-FFF 0°, 15°, 30°, 45°, 60° and 75° printing angles

The properties of the 90° (upright) specimens used in the current paper are taken from our previous ongoing study as reported by Gewelber et al. (2020) [3]. The specimens were produced using the solid mode filling mode with a single outer raster line defining the layer's perimeter; each layer is composed of individual raster lines whose orientation varies between the layer at -45°/+45° (crisscross) according to the print strategy; the crisscross strategy is the most frequently employed as the default raster pattern in most FFF extruders. The build chamber temperature was ~70 ºC; the printing extrusion temperature was ~285 ºC, the nozzle diameter was 0.4 mm, the nominal print speed was 12.7 mm/sec, and the layer thickness was 0.178 mm.

The length of the specimen was measured with an error of 0.02 mm using a digital caliper and its height (h) and width (b) were measured with a micrometer with an error of 0.01 mm. The dimensions and accuracy of the specimens for the 0°, 15°, 30°, 45°, 60° and 75° specimens are presented in table 1. The mass was measured with an error of 0.0001g using an MRC ABS-220-C2 analytical balance.

The absolute density was calculated by dividing the specimen's mass by its volume. Relative density was obtained by dividing the absolute density by the ABS supplier provided density, which is 1.04 gr/cm^3, as presented in table 2.

Table 1. Dimensional accuracy of the FFF-ABS 3D-printed three-point bend test specimens printed at different angles (Fig. 3), where l is specimen's length, and b and h are the measured dimensions of the specimen's cross-section

Average dimension	Different angles configuration					
	0°	15°	30°	45°	60°	75°
l (mm)	127.5±0.0	127.5±0.0	127.4±0.0	127.2±0.0	127.2±0.0	127.3±0.0
h (mm)	12.8±0.1	12.9±0.1	12.9±0.0	12.7±0.1	12.7±0.0	12.7±0.0
b (mm)	3.2±0.0	3.2±0.0	3.2±0.0	3.3±0.0	3.2±0.0	3.2±0.0

Table 2. Average properties of the tilted FFF-ABS specimens (Fig. 3), where ρ_r (%) is the relative density, δ (mm) is the axial deflection, and σ (MPa) is the flexural strength properties. The properties of the 90° (upright) specimens were reported by Gewelber et al. (2020) [3]

Specimen inclination angle	ρ_r [%]	δ [mm]	σ [MPa]
0°	94.8	3.5	63.2
15°	92.7	4.1	61.2
30°	91.8	3.0	49.1
45°	88.8	2.2	34.6
60°	88.1	1.7	26.4
75°	86.6	1.1	18.0
90°	89.1	1.1	22.2

2.2. Mechanical Testing

The three-point bend tests according to ASTM D-790 standards were conducted with a computerized MTS© Model E43-504 universal testing system using a crosshead velocity of 0.5 mm min^{-1}. The machine was equipped with a deflection gage and a bend fixture, and the experimental method included collecting on-line load-deflection data during the test. The axial deflection was measured with an error of 0.02 mm and the load (Newton) with a 0.5% error. The test specimen beam of the rectangular cross-section (12.7 mm × 3.2 mm) was supported by two anvils and the loading nose bent the beam by applying a load centrally between the support anvils (Fig. 4). Flexural strength (FS) was calculated using the formula $\sigma_b = \frac{3FL}{2bh^2}$ where F is the applied force, L is the distance between the two anvils, and b and h are the dimensions of the specimen's cross-section (Fig. 2). The Stratasys data sheet for ABS material used in this study includes the bending properties for two build orientations [19].

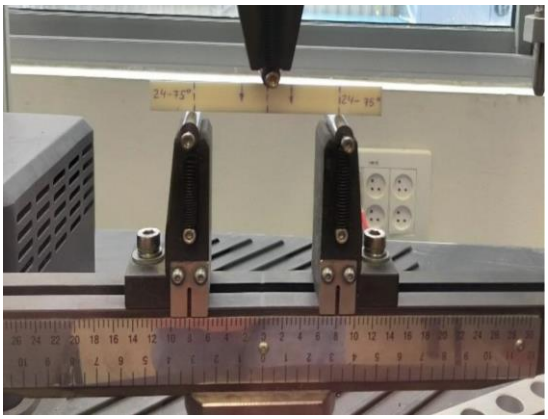

Fig. 4. The MTS© Model E43-504 universal testing system equipped with a bend fixture; and FFF-ABS bend test specimen during the three-point bend tests

2.2. Structure Visualization and Fractographic Methods

Computer-aided design (CAD) visualization modeling of the AM-FFF specimen structure was performed with an Autodesk Inventor 2021 CAD software, based on the theoretically designed dimensions of the printed specimen, and according to the following assumptions: (a) the layered rasters have an elliptical cross-section of 0.43 mm × 0.18 mm, (b) the overlap (penetration) in the model simulates the welds between the adjacent rasters and the size of the overlap, determined by the size of the welds between rasters, (c) there is an overlap between the contour rasters and the adjacent infill rasters, (d) there is an overlap between the adjacent rasters of the same layer (intra-layer bonding), and (e) there is an overlap between the rasters of the adjacent layers (inter-layer bonding), (f) the specimens were printed in the solid mode. Visual testing (VT) inspection combined with a multifocal HIROX RH-2000 3D digital light microscope (LM) and Olympus LEXT OLS410 confocal microscope observation were performed following the mechanical testing, to observe the quality of the printed surfaces, including possible defects, as well as to examine the fracture surface morphology. The HIROX RH-2000 3D LM instrument is equipped with high intensity LED lighting and an improved light sensitivity sensor, displaying high pixel density and low image noise, with an auto-focus and multi-focus system that contains powerful software. The Olympus LEXT OLS4100 is a laser scanning digital microscope equipped with a 405 nm laser for surface observation and measurements at 10 nm resolution. It consists of an optical system and high numerical apertures for non-contact 3D imaging and interpretations.

3. RESULTS

3.1. Dimensional Accuracy and Density

Discontinuities are intrinsic for the current FFF technology since the components are built of deposited ABS filaments having ellipsoidal characteristics that do not pack into an utterly dense volume and do not perfectly bond. Poor bonding zones between rasters inside and in between the layers are commonly observed. Some empty gaps remain between filaments, both in between the layers and within the built layers between rasters. The residual porosity and faulty bonds lead to lower mechanical properties of FFF material when compared to bulk thermoplastic polymer. The macro and microstructural discontinuities play an important role in fracture initiation and cracking, especially in the brittle fracture mode. Typical discontinuities are shown in figure 5 for an upright 45°/+45° crisscross ABS 3D-printed specimen. The tilted specimens dimensions and accuracy and the relative density are reported in table 1 and table 2, respectively. The general view of the outer-surfaces of the tilted ABS crisscross 3D-printed specimens is shown in figure 6.

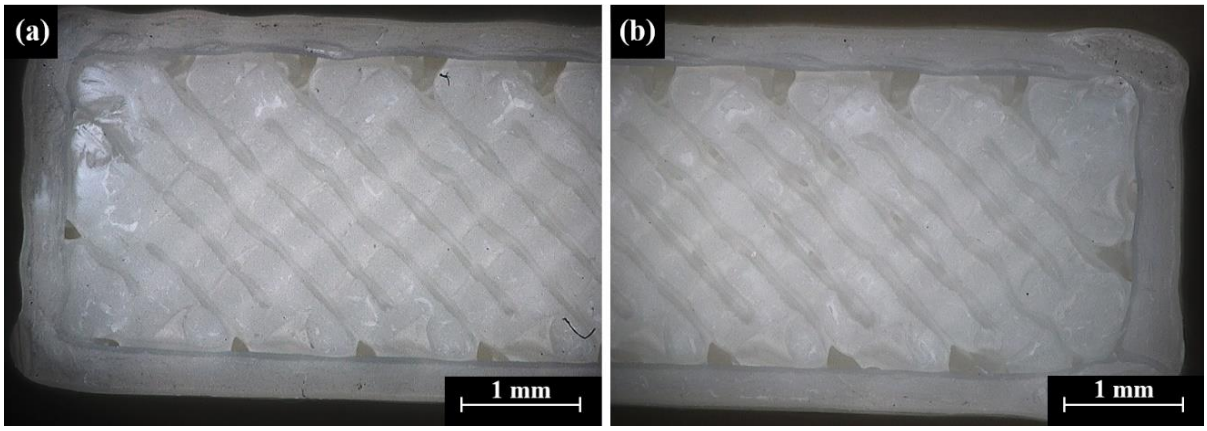

Fig. 5. General view of fracture surfaces of the FFF-ABS 3D-printed specimens for an upright 45°/+45° specimen displaying typical discontinuities: (a) left side of the specimen; and (b) right side of the specimen

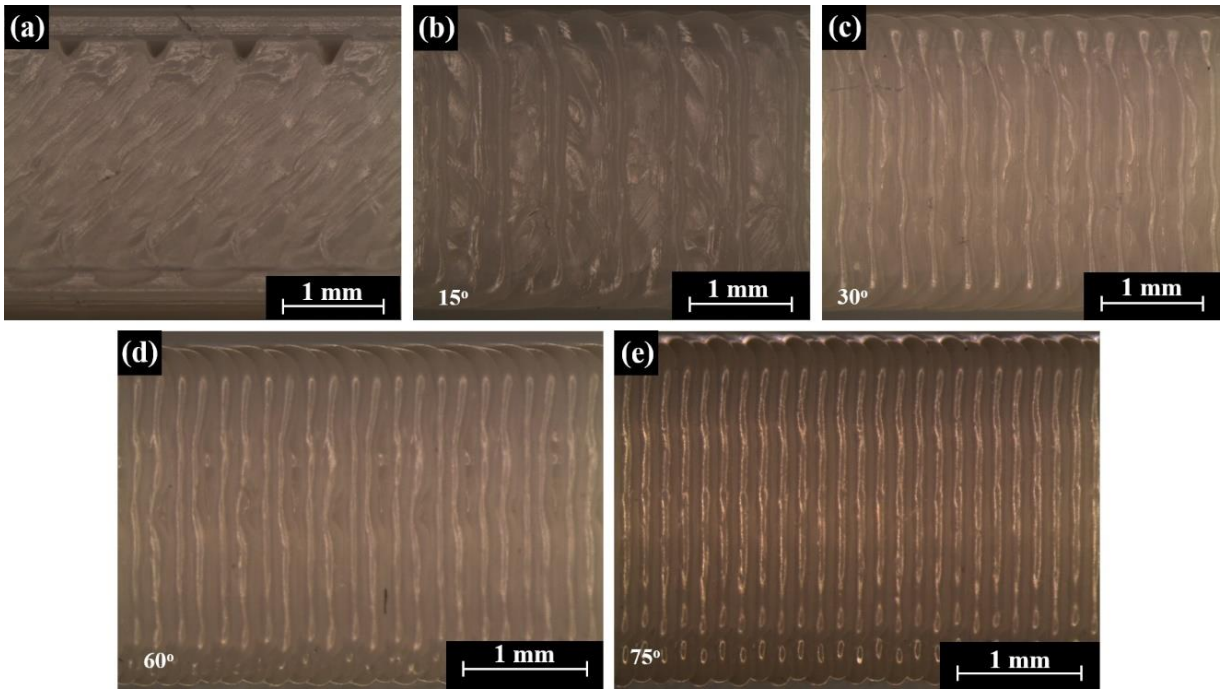

Fig. 6. General view on the outer-surfaces of the tilted FFF-ABS crisscross 3D-printed specimens: (a) on edge (0° tilted) or upright (90° tilted) specimens displaying typical crisscross structure and discontinuities; (b) 15°; (c) 30°; (d) 60°; (e) 75°

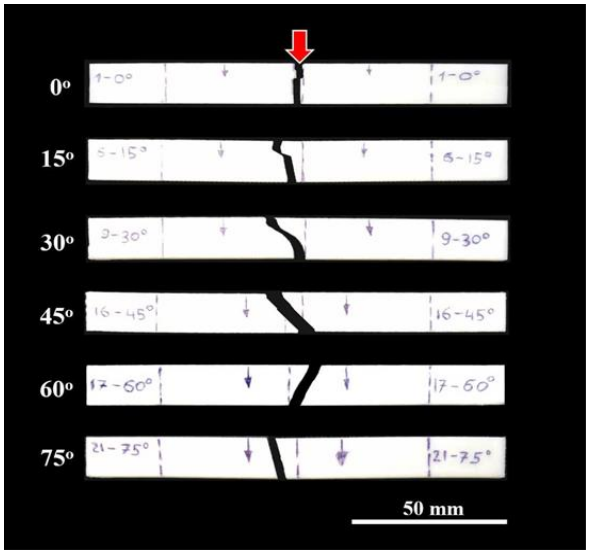

Fig. 7. The FFF-ABS 3D-printed specimens built in various angles: 0°, 15°, 30°, 45°, 60°, 75° (Fig. 3) after they were fractured during the three-point bend test

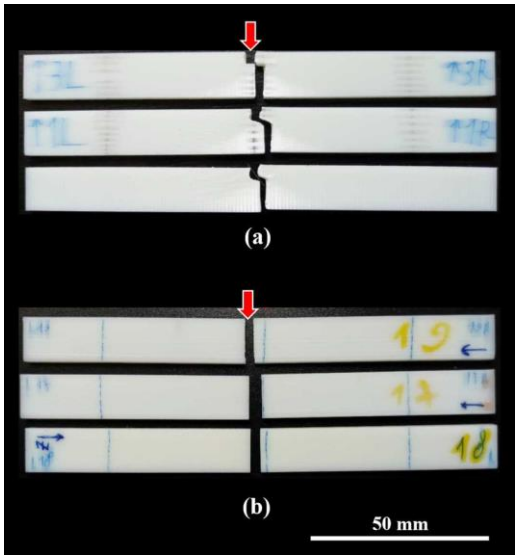

Fig. 8. The FFF-ABS 3D-printed specimens: (a) on-edge (0°) configuration (ρ_r= ~95%); and (b) upright (90°) configuration (ρ_r= ~89%)

3.2. Mechanical Properties

Average mechanical properties of the tilted ABS specimens (Fig. 3), the axial deflection, and the flexural strength, are presented in table 2. The highest values of flexural strength and axial deflection were obtained for the low angle configurations (0° and 15°). The main experimental results of the three-point bend test of specimens built at different angles revealed that the higher the built angle, the smaller the values of the axial deflection and the flexural strength Moreover, as the building angle (relative to the build platform) increases, both maximum bending load and deflection reduce roughly linearly.

3.3. Fractography and Structure Visualization

General view of the crack path for ABS 3D-printed

specimens built at various angles: 0°, 15°, 30°, 45°, 60°, 75° after the three-point bend test are presented in figure 7.

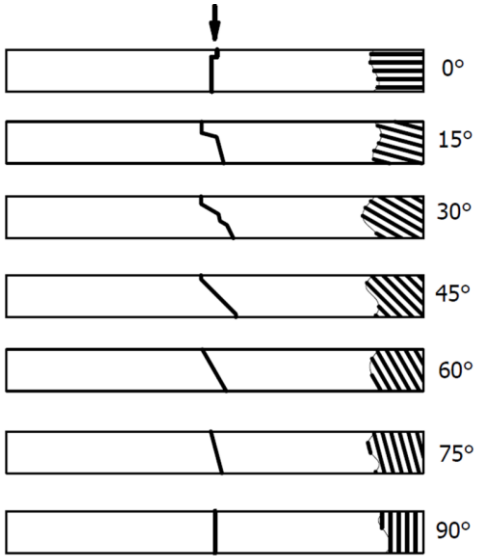

Fig. 9. Schematic-drawing of the crack path for various printing angles: 0°, 15°, 30°, 45°, 60°, 75° (Fig. 3) after three-point bend test

The crack path of 0° and 15° configurations shows a step exhibiting the cantilever (curl) phenomenon (Figs. 7 and 8a), while the 60°, 75° and 90° configurations display a straight path during the three-point bend tests (Figs. 7 and 8b). For 45°, 60°, 75° and 90° configurations, the crack path is in the same direction as the printed layers (parallel to the layer direction); it propagates and cuts the bond between two adjacent layers and exhibits a relatively smooth morphology of fracture surface, typical for brittle fractures (Figs. 7 and 9). For 0°, 15° and 30° configurations, the fracture surface has a relatively rough ductile morphology. A schematic-drawing of the crack propagation during the three-point bend tests of ABS 3D-printed specimens built at different angles is shown in figure 9.

The left and right fracture surfaces and the fracture initiation area of the 15°, 30° and 75° specimens are shown in figures 10, 11, 12, respectively. Bright areas indicating bonding between two adjacent layers and gray gloss areas indicating the lack of bounding were observed at the fracture surface after the three-point bend test (Figs. 10, 11, specimen nos. 8-15° and 11-30°, respectively). Printing defects, such as voids, were also observed (Fig. 12, Specimen no. 21-75°).

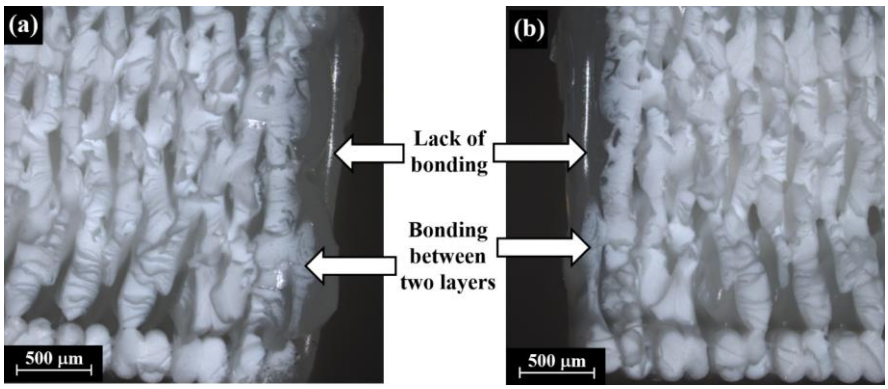

Fig. 10. Fracture initiation location of Specimen no. 8-15°. The whitish areas indicate bonding between two adjacent layers; the gray gloss zones are areas without bonding: (a) the left side of the fractured specimen; and (b) the right side of the fractured specimen

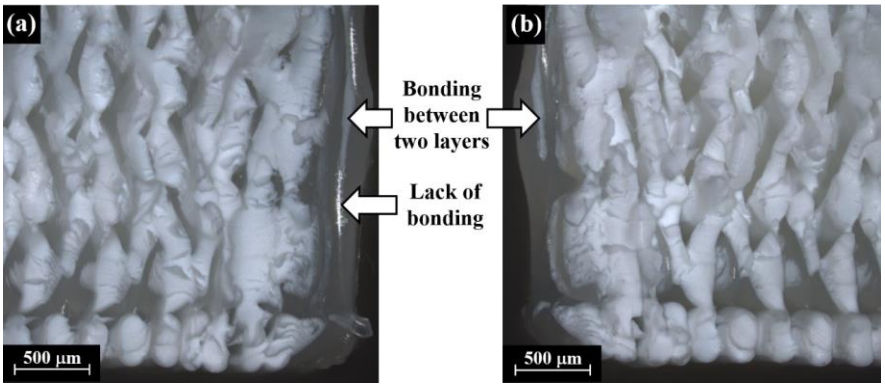

Fig. 11. Fracture initiation location of Specimen no. 11-30°. The whitish areas indicate bonding between two adjacent layers; the gray gloss zones are areas without bonding: (a) the left side of the fractured specimen; and (b) the right side of the fractured specimen

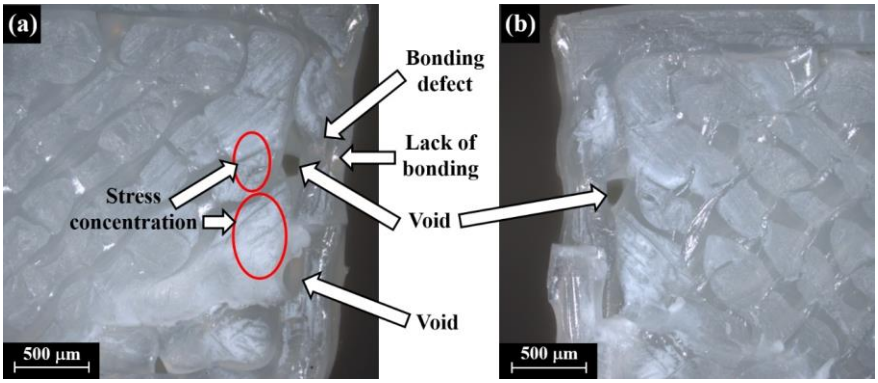

Fig. 12. Fracture initiation location of Specimen no. 21-75°: (a) the left side of the fractured specimen; and (b) the right side of the fractured specimen

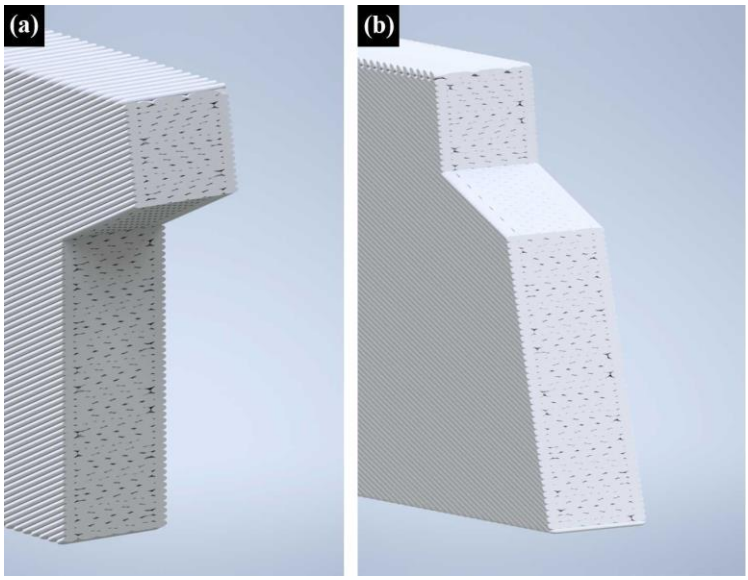

Fig. 13. CAD visualization of the fracture morphology for FFF-ABS specimen printed at 15° (according to Figs. 3, 7 and 9)

The CAD model visualization of 15° configuration (Fig. 13) illustrates the typical crack path and fracture surface. It also shows the start location of the crack, its profile and infill rasters cross-section at the fracture surface, and the crack's path direction change at the end of a fracture (cantilever curl).

4. DISCUSSION

4.1. Mechanical Properties

Three-point bend test was currently used since it generates tension on the low surface, opposite to the load application side, and compression on the other surface of the specimen, producing a gradient in stress through the thickness of the sample. This causes the fracture surface to exhibit important characteristics that are different from fracture surfaces produced in uniaxial tension and in four-point bend method. The flexural test tilted specimens were produced using the crisscross print strategy in order to have the printed fibers arranged in a denser manner; the printed fiber orientation and bond configuration make the specimens capable of better withstanding the flexural load.

The experimental results show that FS and deflection change significantly for the specimens printed at different angles to the build platform (0°, 15°, 30°, 45°, 60°, and 75°) (Table 2). The largest difference is between 0° and 75°/90°, i.e., the FS and the deflection are the largest for the 0° and 15° orientations, followed by the 30°, 45°, 60°, and 75° orientations in descending order. Each of the examined angles exhibits a different pattern of crack propagation during the three-point bend test (Figs. 7, 8, 9). The interlayer strengths of parts generated by FFF-ABS technique suffer due to poor interlayer contact and insufficient diffusion. As expected, the high-angle specimens fail by interlaminar crack propagation, while the failure of the specimens tilted in-between the 15° and 60° range is a consequence of

mixed cross laminar and interlaminar cracking. The low-angle specimens fail mainly by intra-layer crack propagation (Figs. 7 and 8).

4.2. Fractography and Structure Visualization

For specimens printed at 0°, 15° and 30° orientations, a symmetric pattern of straight lines with different lengths was observed on both sides of the crack propagation path. The lines are located at equal distances from each other and have different lengths, forming a triangular pattern, about 10 mm on each side of the fracture. Each pattern has a triangular shape with the base at the lower side of the specimen (where the tensile stress has the maximum value), and a vertex directed toward the neutral plane of a bending. The length of lines probably indicates the intensity of bending stresses in different cross-sections along the specimen. The maximum bending stress develops in a section with maximum bending moment value, so in this section the line has the maximum length, and it decreases while moving away from the cross-section with maximum bending moment. These lines are the evidence of a crazing polymer phenomenon and are the visual expression of the stress field magnitude and distribution around the fracture location.

During a three-point bend test, the maximum bending stress develops in the cross-section of the applied load; therefore, it was expected that the crack would start in this cross-section. However, in some specimens the crack starts a few millimeters away from this section (Figs. 7 and 8) because it begins, due to energetic considerations, at the weakest inter-layer bonding zone, containing inter-laminar discontinues serving as stress concentration points.

During microscopic examination of crack initiation regions of some specimens (nos. 8-15°,11-30°, 21-75°) it was found that there is a very small bonding area between two adjacent profile rasters, and a large area without bonding at all (void) (Fig. 10, Specimen no. 8-15°, Fig. 11, Specimen no. 11-30°). In this case, the tension stress at this section is distributed over a relatively small area of bonding zone, causing stress to obtain greater values than in other cross-sections. As a result, a crack starts to propagate in the cross-section with the maximum local tension stress away from the applied load cross-section. In the case of Specimen no. 21-75°, there are some defects of bonding between two adjacent profile rasters at the crack start zone; some of them occasionally initiated a local intra-layer crack that crosses from initial layer to adjacent one. In addition, there are relatively large voids between infill and profile rasters, surrounded by visible stress concentration fields (crazing) (Fig. 12).

The three-point bend test produces shear stresses in addition to tensile stresses. Tensile stress develops in the direction perpendicular to the plane of the crack, and shear stress develops parallel to the plane of the crack. Thus, during bending the crack develops in a combined mode: opening mode and in-plane shear (sliding) mode (Mode I + Mode II). As a result, the equivalent stress that causes the crack to open, develops at a certain angle to the tensile stress (applied load cross-section). Because the shear stress magnitude is much smaller than the tensile stress magnitude, the shear stress does not affect the direction of crack development for brittle specimens (45°, 60°, 75° and 90°), if relatively little energy is required for crack propagation through the weakest zones (through the bonds between two adjacent layers). During the bending of relatively ductile specimens (0°, 15° and 30°) they are able to accumulate relatively great energy. As a crack propagates, the cross-sectional area of a specimen decreases and the force acting on it increases, resulting in an increase of equivalent stress magnitude. As soon as a crack reaches a point where it can propagate through a weaker material (bonding between two layers), under the influence of the equivalent stress, it sharply changes its direction, thus creating a lip or curl located in the compression side, that is commonly called cantilever curl. The CAD model visualization of a typical cantilever curl of the 15° configuration specimen is shown in Fig. 13. In the future, a CAD model of other cantilever curl angles, in addition to the 15° configuration, should be examined.

4. CONCLUSIONS

The current study focuses on the relationship between the process parameters and mechanical properties of AM-FFF ABS parts.

The overall evaluation of the mechanical strength values of the tilted specimens shows clearly that much higher mechanical properties (flexural strength and deflection) are to be expected for specimens printed at the low angle orientations. Considering applications of 3D printed parts in varied industries, this comparative study demonstrates the possible advantages of employing the low angle and on-edge orientations in FFF printed load bearing parts.

This study is part of an ongoing project examining the AM FFF-ABS mechanical properties. In a future study it is recommended to add design calculations in order to support the choice of the AM FFF-ABS process parameters. In addition, it is suggested to examine the influence of the thermal gradient existing between the top and bottom gradient on the material properties.

The tested tensile specimens revealed two main failure modes: (1) inter-layer/ inter-raster bond failure is typical for upright specimens; and (2) intra-layer/trans-raster failure is typical for on edge specimens. In addition, a mixed inter-layer/ intra-layer mode was found for the specimens tilted in between the 15^{o} and 60^{o} range.

The suggested methodology used here for the examination of FFF-ABS specimens could be used for the study of other AM-FFF polymers used for 3D-printing.

ACKNOWLEDGEMENTS

The authors would like to thank A. Ulanov, N. Dresler, S. Maman, and N. Bilenkin, from the School of Mechanical Engineering, Afeka Academic College of Engineering, for their engineering and technical assistance. Thanks, are also due to D. Sherman from the School of Mechanical Engineering, Tel Aviv University for his valuable contributions. The authors are also grateful to Barbara Doron for the English editing.

REFERENCES

[1] **Popescu D., Zapciu A., Amza C., Baciu F., Marinescu R.,** *FDM process parameters influence over the mechanical properties of polymer specimens: A review*, Polymer Testing 69, 2018, pp. 157–166.

[2] **Cuan-Urquizo E., Barocio E., Tejada-Ortigoza V., Pipes R. B., Rodriguez C. A., Roman-Flores A.,** *Characterization of the mechanical properties of FFF structures and materials: A review on the experimental, computational and theoretical approaches*, Materials 12, 2019, p. 895.

[3] **Gewelber O., Rosenthal Y., Ashkenazi, D., Stern A.,** *Mechanical Properties, Structure and Fracture Behavior of Additive Manufactured FFF-ABS Specimens*, Annals of "Dunarea de Jos" University of Galati. Fascicle XII, Welding Equipment and Technology 31, 2020, pp. 71–78.

[4] **Pranzo D., Larizza P., Filippini D. and Percoco G.,** *Extrusion-based 3D printing of microfluidic devices for chemical and biomedical applications: A topical review*, Micromachines 9, 2018, p. 374.

[5] **Algarni M., Ghazali S.**, *Comparative Study of the Sensitivity of PLA, ABS, PEEK, and PETG's Mechanical Properties to FDM Printing Process Parameters*, Crystals 11(8), 2021, p. 995.

[6] **Goh G. D., Yap Y. L., Tan H. K. J., Sing S. L., Goh G. L., Yeong W. Y.**, *Process–structure–properties in polymer additive manufacturing via material extrusion: A review*, Critical Reviews in Solid State and Materials Sciences, 45, 2020, pp. 113–133.

[7] **Garzon-Hernandez S., Arias A., Garcia-Gonzalez D.**, *A continuum constitutive model for FDM 3D printed thermoplastics*, Composites Part B: Engineering 201, 2020, p. 108373.

[8] **Khosravani M. R., Berto F., Ayatollahi M. R., Reinicke T.**, *Fracture behavior of additively manufactured components: A review*, Theoretical and Applied Fracture Mechanics 109, 2020, p. 102763.

[9] **Verma P., Ubaid J., Schiffer A., Jain A., Martínez-Pañeda E., Kumar S.**, *Essential work of fracture assessment of acrylonitrile butadiene styrene (ABS) processed via fused filament fabrication additive manufacturing*, The International Journal of Advanced Manufacturing Technology 113(3), 2021, pp. 771–784.

[10] **Sheoran A. J., Kumar H.**, *Fused deposition modeling process parameters optimization and effect on mechanical properties and part quality: Review and reflection on present research*, Materials Today: Proceedings 21, 2020, pp. 1659–1672.

[11] **Vanaei H. R., Raissi K., Deligant M., Shirinbayan M., Fitoussi J., Khelladi S., Tcharkhtchi A.**, *Toward the understanding of temperature effect on bonding strength, dimensions and geometry of 3D-printed parts*, Journal of Materials Science, 55(29), 2020, pp. 14677–14689.

[12] **Coasey K., Hart K. R., Wetzel E., Edwards D., Mackay M.E.**, *Nonisothermal welding in fused filament fabrication*, Additive Manufacturing 33, 2020, p. 101140.

[13] **Coogan T. J., Kazmer D. O.**, Prediction of interlayer strength in material extrusion additive manufacturing. Additive Manufacturing 35, 2020, p. 101368.

[14] **Dundar M. A., Dhaliwal G. S., Ayorinde E.**, *Experimental and numerical investigation on flexural behavior of acrylonitrile-butadiene-styrene polymer*, Polymer Engineering & Science 60(11), 2020, pp. 2930–2944.

[15] **Dundar M. A., Dhaliwal G. S., Ayorinde E., Al-Zubi M.**, *Tensile, compression, and flexural characteristics of acrylonitrile–butadiene–styrene at low strain rates: Experimental and numerical investigation*, Polymers and Polymer Composites 29(5), 2021, pp. 331–342.

[16] **Shabat D., Rosenthal Y., Ashkenazi D., Stern A.**, *Mechanical and structural characteristics of fused deposition modeling ABS material*, Annals of "Dunarea de Jos" University of Galati. Fascicle XII, Welding Equipment and Technology 28, 2017, pp. 16–24.

[17] **Solomon A., Rosenthal Y., Ashkenazi D., Stern A.**, *Structure and mechanical behavior of additive manufactured fused deposition modeling ABS*, Annals of "Dunarea de Jos" University of Galati. Fascicle XII, Welding Equipment and Technology 29, 2018, pp. 47–56.

[18] **Ahmed S. W., Hussain G., Altaf K., Ali S., Alkahtan M., Abidi M. H., Alzabidi, A.**, *On the effects of process parameters and optimization of interlaminate bond strength in 3D printed ABS/CF-PLA composite*. Polymers 12(9), 2020, p. 2155.

[19] ***, http://www.stratasys.com/-/media/files/material-spec-sheets/mss_fdm_absplusp430_1117a.pdf